The Potential of a Separated Electric Compound Spark-Ignition Engine for Hybrid Vehicle Application

Emiliano Pipitone[1]
Department of Engineering,
University of Palermo,
Viale delle Scienze, Edificio 8,
Palermo 90128, Italy
e-mail: emiliano.pipitone@unipa.it

Salvatore Caltabellotta
Department of Engineering,
University of Palermo,
Viale delle Scienze,
Palermo 90128, Italy
e-mail: salvatore.caltabellotta@unipa.it

In-cylinder expansion of internal combustion engines based on Diesel or Otto cycles cannot be completely brought down to ambient pressure, causing a 20% theoretical energy loss. Several systems have been implemented to recover and use this energy such as turbocharging, turbomechanical and turbo-electrical compounding, or the implementation of Miller cycles. In all these cases however, the amount of energy recovered is limited allowing the engine to reach an overall efficiency incremental improvement between 4% and 9%. Implementing an adequately designed expander–generator unit could efficiently recover the unexpanded exhaust gas energy and improve efficiency. In this work, the application of the expander–generator unit to a hybrid propulsion vehicle is considered, where the onboard energy storage receives power produced by an expander–generator, which could hence be employed for vehicle propulsion through an electric drivetrain. Starting from these considerations, a simple but effective modeling approach is used to evaluate the energetic potential of a spark-ignition (SI) engine electrically supercharged and equipped with an exhaust gas expander connected to an electric generator. The overall efficiency was compared to a reference turbocharged engine within a hybrid vehicle architecture. It was found that, if adequately recovered, the unexpanded gas energy could reduce engine fuel consumption and related pollutant emissions by 4–12%, depending on overall power output. [DOI: 10.1115/1.4053393]

Keywords: hybrid vehicle, compound engine, spark-ignition engine, exhaust energy recovery

Introduction

Regulations adopted worldwide to reduce the environmental impact of human activities force the development of market solutions capable of increasing fuel economy and respecting the environment. Among the various solutions, hybrid electric vehicles including plugin varieties are a promising solution, showing significant fuel consumption reduction compared to traditional internal combustion engine vehicles, mainly in urban applications. Hybrid electric vehicles have a relatively short history and their developmental stage is undoubtedly open to relevant improvements. Among interventions, the internal combustion engine is a key element with room for modifications and improvements [1]. One example is reducing the exhaust gas energy loss related to incomplete gas expansion inside the cylinder of engine operating according to the Diesel or Otto thermodynamic cycles. As an example, the dashed area 4–6–1–4 in Fig. 1 represents the energy loss related to the unexpanded gas in an Otto cycle.

Several systems have been studied and proposed to recover or use unexpanded gas energy in engines, the most common being represented by turbocharging. In this case, the turbine recovers only the energy required by the turbocompressor, thus considerably limiting the recovery amount. Several other systems can be traced in the scientific literature [2,3]. Turbocompounding, as an example, was widely adopted in the naval propulsion sector, employing a second turbine downstream the first to complete the exhaust gas expansion, thus adding power to the propeller shaft and increasing fuel economy. In the automotive sector, several versions of turbocompounding have been proposed. In some cases, usually indicated as "electrical turbocompound," an electrical generator installed on the turbocharger shaft was controlled to recover the residual power produced by the turbine not employed by the turbocompressor [4–7]. Results generally show that overall engine efficiency cannot be increased more 6%. In other cases, an auxiliary turbogenerator was installed downstream of the first turbine [8,9], reaching a maximum fuel economy improvement of 4%. A different version has also been proposed [10,11], with an auxiliary turbogenerator installed in parallel to the turbine of the turbocharger. Experiments with both fixed and variable geometry turbines have shown efficiency improvements up to 9%.

Another possible solution for greater exploitation of in-cylinder gas expansion to increase efficiency is to adopt overexpanded cycles, such as Atkinson and Miller cycles [12]. According to the Atkinson cycle (1–2–3–6–1 in Fig. 1), gas expansion should be prolonged down to atmospheric pressure [13–15], thus completely recovering both the dashed areas of Fig. 1. Full expansion could be practically obtained by adopting adequate intake valve phasing. The theoretical efficiency increment compared to Otto cycle with the same compression ratio (CR) is around 19%. However, an extremely large and impractical in-cylinder volume would be necessary. The Atkinson cycle engine displacement is approximately four times the Otto cycle displacement, which strongly decreases the engine's power density (indicated mean effective pressure (IMEP) reduction in the order of −72%). In the Miller cycle, the expansion stroke is prolonged while maintaining plausible in-cylinder volumes, thus reaching a final expansion pressure p_5 substantially higher than atmospheric pressure [16]. This can be practically pursued by adopting high engine CR and early (or late) intake valve closure (IVC) to limit the compression stroke and exploit the full expansion stroke [11].

By adopting a CR of 14, an 8% theoretical efficiency increment can be obtained with respect to the Otto cycle, to the detriment of
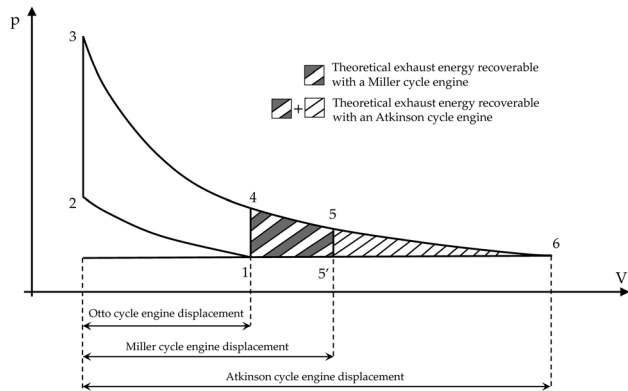

Fig. 1 Comparison between Otto, Miller, and Atkinson cycle

power density, which is reduced by about 25%. A practical realization is represented by the Toyota Prius hybrid vehicle, which implements a Miller cycle engine with a CR of 13, achieving a fuel economy improvement of 8.5% [17]. Although the implementation of the Miller cycle can achieve good fuel consumption improvement, the resulting power density reduction still represents a crucial drawback that limits its advantage [18].

An alternative approach for recovery and utilization of the unexpanded gas energy is presented in this paper. A separated electric compound system is considered that involves an exhaust gas expander connected to an electric generator and a supercharger driven by an electric motor. The system proposed has the potential to increase the vehicle efficiency over a wide range of operating conditions.

Compound Engine Concept Description

The powertrain architecture considered in this work is given as type (a) in Fig. 2. Unlike other studied electric compound systems (types (b) and (c) in Fig. 2), the two thermal machines (compressor C and expander E) operate independently in the system considered here. Each one is connected to its own electric machine, and the exhaust gas expander operates at high pressure directly downstream of the thermal engine [2]. The compound system presented in this paper is hence composed of an electrically supercharged spark-ignition (SI) engine whose exhaust gas flows through a properly designed exhaust gas expander (E) connected to an electrical generator (G). The system is specifically intended for a hybrid propulsion architecture application [19], where the onboard storage system may receive and store the energy produced by the expander–generator group. This energy can then be employed for vehicle propulsion. Moreover, in a hybrid propulsion system, the thermal engine is not involved throughout the wide and rapidly changing operating conditions of a traditional vehicle. Therefore, the exhaust gas expander could be used under quasi-steady conditions and hence near-maximum expansion efficiency. For this reason, the compound engine (CE) considered in this paper is particularly suitable for applying to thermal-electric hybrid propulsion systems.

Figure 3 shows a possible hybrid propulsion layout that includes the compound engine concept. The net power produced by the expander–generator is summed to the power delivered by the thermal engine–generator (MG1) in the energy storage system, which, in turn, supplies the second electric machine (MG2) and the motor–compressor employed for supercharging purposes. It is worth mentioning that in the system described, the expander–generator is always active in conjunction with the thermal engine, contributing to the energy balance of the whole vehicle. However, the motor–compressor unit is powered only when supercharging is required, i.e., only when higher engine loads are required.

In this paper, the authors aim to evaluate the efficiency improvements obtainable by the proposed separated compound
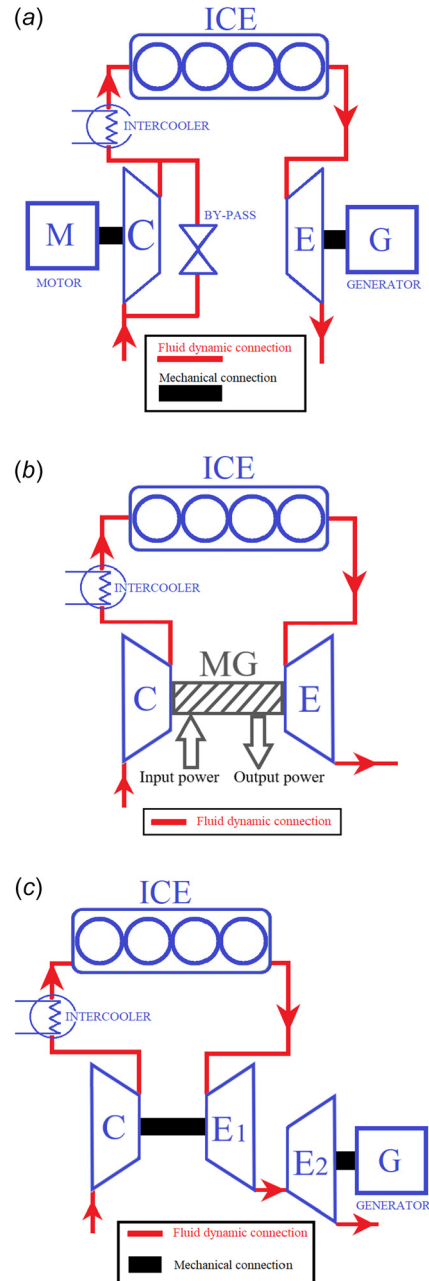

Fig. 2 Electric compound system [2]: (a) separated electric compound; (b) high-pressure electric compound; and (c) low-pressure electric compound (C = compressor; E = exhaust gas expander; M = electric motor; G = electric generator; and ICE = internal combustion engine)

electric engine in comparison with a traditional turbocharged engine for hybrid vehicle applications. For this purpose, a performance comparison was conducted between the CE and a reference turbocharged engine through a simple modeling approach. Fundamentally, the approach consists of mass flow and power balance equations, accompanied by simplifying assumptions and relations. The theoretical approach was also supported by experimental data derived from relevant scientific literature or directly measured through experiments. Focusing on the hybrid vehicle application, the comparison considered only steady-state conditions and was carried out on an equal output power basis; all the propulsive units were sized for the same maximum output power of 73.5 kW (i.e., 100 hp).

The concept described here is novel, as there is no evidence of a study like the one presented here in the scientific literature.
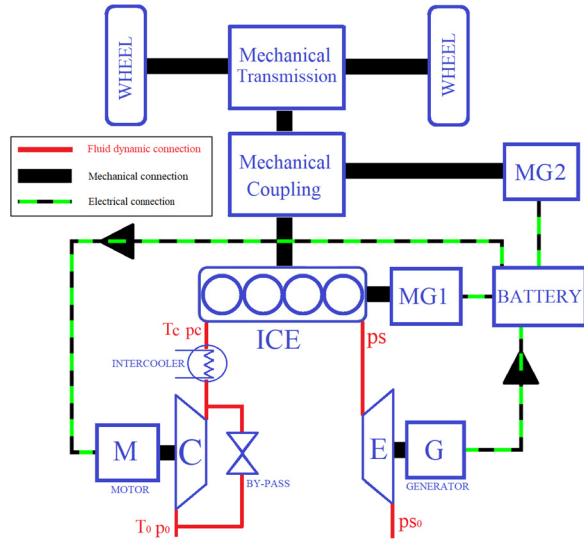
Fig. 3 Hybrid propulsion system endowed of the proposed compound engine (C = compressor; E = expander; ICE = internal combustion engine; M = electric motor; G = electric generator; and MG1 and MG2 = motor–generator units)

Although the separated electric CE has been cited in Ref. [20] among several other different systems that could be simulated, its advantages in terms of overall efficiency were not evaluated, nor were its performances compared to a traditional internal combustion engine.

Baseline Naturally Aspirated Engine

To perform a fair comparison, the authors decided to evaluate the performance of both the electric CE and the comparative turbocharged engine starting from a common baseline naturally aspirated engine. As the first step, the steady-state performances of the baseline naturally aspirated engine were delineated. The authors employed the experimental data reported in Ref. [21], which were obtained on a gasoline variable valve timing (VVT) SI engine. Considering the application of the analyzed propulsion system to a plausible European Type C–Medium hybrid vehicle, the performances reported in Ref. [21] were adapted to a mid-level passenger car engine using a normalization procedure. For that purpose, the normalized mean piston speed u was employed

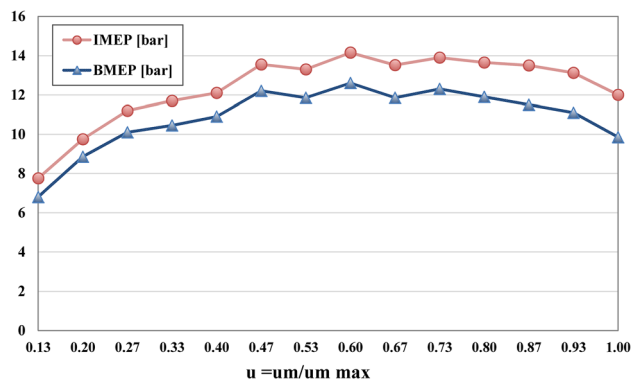$$u = \frac{u_m}{u_{m,\max}} \quad (0 \leq u \leq 1) \tag{1}$$

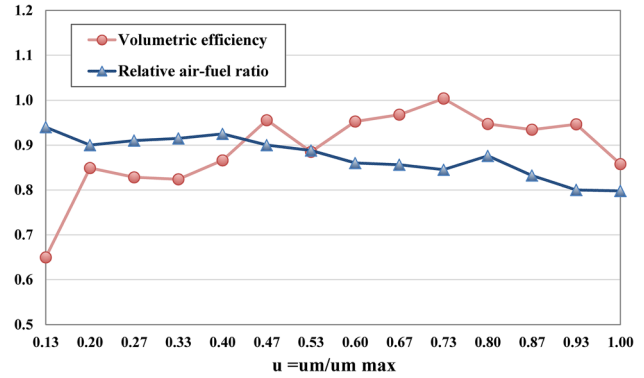**Fig. 4 BMEP and IMEP as a function of the normalized mean piston speed at full load**

Fig. 5 Full load volumetric efficiency and relative air–fuel ratio as a function of the normalized mean piston speed

As a result, Figs. 4 and 5 show the resulting values of:

(1) brake mean effective pressure (BMEP)
(2) indicated mean effective pressure (IMEP)
(3) relative air–fuel ratio (λ)
(4) volumetric efficiency (λ_V)

as functions of the normalized mean piston speed and for the full load condition. Figure 6 presents the BMEP as a function of the manifold absolute pressure (MAP), which is the engine load control parameter for a fixed normalized mean piston speed.

Regarding the overall mechanical efficiency η_m is represented by the following equation:

$$\eta_m = \frac{\text{BMEP}}{\text{IMEP}} = \frac{\text{IMEP} - \text{FMEP}}{\text{IMEP}} = 1 - \frac{\text{FMEP}}{\text{IMEP}} \tag{2}$$

The Chen–Flynn model was followed in the calculation. The friction mean effective pressure (FMEP) was considered a function of the IMEP, used here in place of the maximum in-cylinder pressure as the pressure-load related variable and of the normalized mean piston speed u

$$\text{FMEP} = A + B \cdot \text{IMEP} + C \cdot u + D \cdot u^2 \tag{3}$$

Therefore, the overall mechanical efficiency η_m is

$$\eta_m = 1 - \frac{A + B \cdot \text{IMEP} + C \cdot u + D \cdot u^2}{\text{IMEP}} \tag{4}$$

The mechanical friction model A, B, C, and D parameters were determined using a least-squares regression performed employing the experimental BMEP and IMEP data of Figs. 4 and 6.

For the baseline naturally aspirated engine, the full load IMEP values reported in Fig. 4 were entirely adopted, while the BMEP
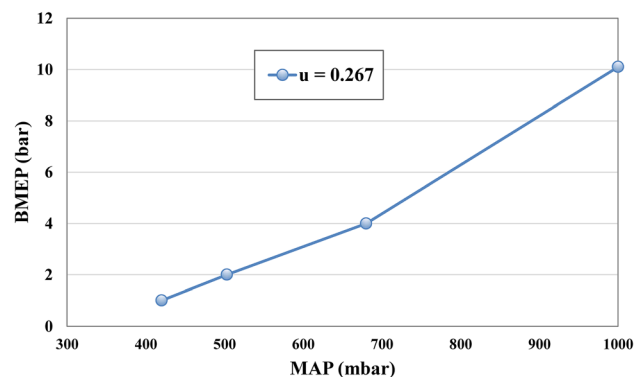

Fig. 6 Brake mean effective pressure as a function of manifold absolute pressure at $u = 0.267$

Table 1 Parameters determined for the Chen and Flynn FMEP model

A (bar)	0.63043
B	0.039807
C (bar)	−0.058036
D (bar)	1.05804

value, for each speed and load, was obtained by the application of the FMEP model of Eq. (3) using the parameters of Table 1

$$\text{BMEP} = \text{IMEP} - \text{FMEP} \quad (5)$$

Concerning the air–fuel ratio, a stoichiometric mixture (i.e., $\lambda = 1$) was assumed with MAP up to 0.9 bar, being the stoichiometric air–fuel ratio $\alpha_{st} = 14.7$ for gasoline; for the higher loads (i.e., MAP > 0.9 bar), the usual air–fuel enrichment performed on gasoline SI engine to avoid knocking phenomena was adopted, assuming a linear variation with MAP up to the full load values (already reported in Fig. 5 for each normalized mean piston speed).

Taking into consideration the parameters which contribute to defining the BMEP

$$\text{BMEP} = \frac{\delta_0 \cdot \lambda_V \cdot \text{LHV}}{\lambda \cdot \alpha_{st}} \cdot \eta_i \cdot \eta_m \quad (6)$$

and considering the manifold air density δ_0 at the ambient conditions $p_0 = 1$ bar and $T_0 = 288$ K ($\Rightarrow \delta_0 = 1.209$ kg/m³) together with an average gasoline lower heating value LHV of 43 MJ/kg, it was possible to determine the engine indicated efficiency η_i for each load (i.e., BMEP) normalized mean piston speed, and the brake thermal efficiency η_b

$$\eta_b = \eta_i \cdot \eta_m \quad (7)$$

as well as the brake specific fuel consumption BSFC

$$\text{BSFC}_{(g/kWh)} = \frac{3600}{\text{LHV}_{(MJ/kg)} \cdot \eta_b} = \frac{\delta_{0\,(kg/m^3)} \cdot \lambda_V \cdot 36,000}{\text{BMEP}_{(bar)} \cdot \lambda \cdot \alpha_{st}} \quad (8)$$

Given the full load BMEP curve shown in Fig. 4, with a maximum value of 12.6 bar, the engine was sized considering the target output power of 73.5 kW. The required displacement V_A of the naturally aspirated baseline engine was 1352 cc. In line with current passenger car engines, a maximum mean piston speed of 17 m/s was adopted for each engine considered in this study: this is equivalent to assuming that the different engines share the same technology level, hence the same mechanical performance.

With values obtained for thermal efficiencies, the volumetric CR reported in Ref. [21] was assumed for the baseline engine. The value of 1.11 was assumed for the stroke-to-bore ratio for

Table 2 Main characteristics of the gasoline SI baseline engine

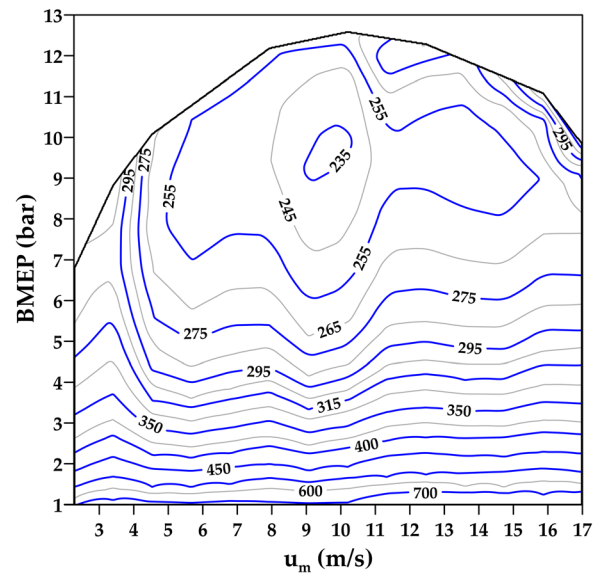| Engine	Four-stroke, naturally aspirated, spark ignition
Displacement	1352 cc
Number of cylinders	4
Bore	72.9 mm
Stroke	80.9 mm
Maximum mean piston speed	17 m/s
Compression ratio	11
Injection system	Multipoint
Valvetrain	Four valves/cylinder, VVT
Maximum BMEP	12.6 bar at 3780 rpm
Maximum power	73.5 kW at 5880 rpm
Minimum BSFC	232.9 g/kWh

Fig. 7 Brake specific fuel consumption map of the baseline naturally aspirated engine

each engine model presented in this paper, as is the average and typical value adopted on current engines employed in hybrid propulsion vehicles. For passenger car engines, the displacement of a single cylinder is typically approximately 0.5 L in a four cylinder layout. These dimensions were chosen for the baseline engine, whose main characteristics are presented in Table 2. The contour map of the BSFC obtained for the baseline SI engine is reported in Fig. 7 as a function of mean piston speed u_m and BMEP.

Reference Turbocharged Engine

As already mentioned, the advantages of implementing the separated electric compound SI engine were evaluated by comparing it with a reference traditional turbocharged engine. In this section, the authors describe the calculations carried out to determine the size and performance of the turbocharged reference engine, which is schematically represented in Fig. 8. As can be observed, a waste-gate valve was considered for the turbine bypass, and an intercooler between the engine and compressor was assumed to cool down the air charge. The BMEP of the turbocharged engine was evaluated based on the specific performance and parameters of the Baseline Naturally Aspirated Engine, delineated in the section, and assuming a maximum allowed boost pressure of 1.5 bar (absolute).

The specific performance of the turbocharged engine can be evaluated starting from the air mass flow to the engine G_C, which
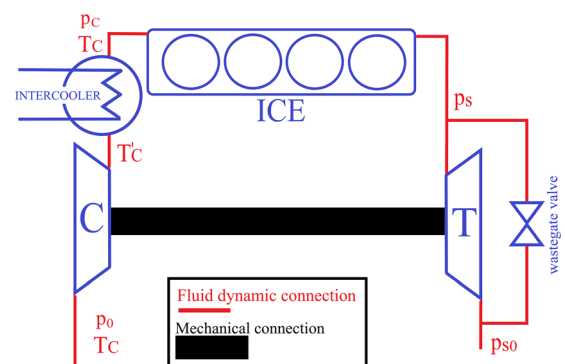

Fig. 8 Schematic representation of the turbocharged baseline engine (C = compressor; T = turbine; and ICE = internal combustion engine)

depends on the mean piston speed u_m and the manifold pressure MAP

$$G_C = \frac{V_T \cdot n}{60 \cdot \varepsilon} \cdot \delta_C \cdot \lambda_{V,C} \frac{\alpha}{\alpha + \frac{1}{\delta'}} \qquad (9)$$

where δ_C is the air density in the manifold, $\lambda_{V,C}$ is the turbocharged engine volumetric efficiency, n is the engine speed, V_T is the turbocharged engine displacement, and δ' is the relative fuel density, i.e., the ratio between fuel and air density

$$\delta' = \delta_F/\delta_A \qquad (10)$$

The air density depends on the manifold absolute pressure MAP and the intercooler outlet temperature T_C

$$\delta_C = \frac{\text{MAP}}{R' \cdot T_C} \qquad (11)$$

In the calculation, gasoline was assumed to enter the cylinder with 40% of the mass already evaporated; this allowed evaluating the average fuel density δ_F as

$$\delta_F = \delta_{F,V} \cdot 0.4 + \delta_{F,L} \cdot 0.6 \qquad (12)$$

where $\delta_{F,L}$ and $\delta_{F,V}$ are the fuel densities in the liquid and vapor phase, respectively. The latter was determined utilizing the perfect gas law adopting the molecular mass of 100 g/mol for the gasoline [22].

It is worth noting that the MAP may differ from the compressor outlet pressure p_c due to the necessary gas throttling at part load. Assuming an intercooler efficiency R_{INT} of 0.7, the gas temperature at the intercooler outlet was evaluated as

$$T_C' = T_0 \cdot \left(1 + \frac{\beta_C^{\frac{k_c-1}{k_c}} - 1}{\eta_C} \right) \qquad (13)$$

$$T_C = T_C' - R_{\text{INT}}(T_C' - T_0) \qquad (14)$$

where the compressor outlet temperature T_C' was calculated in Eq. (13) as a function of the compression ratio $\beta_C = p_C/p_0$, of the air isentropic coefficient k_c and compressor adiabatic efficiency η_C (whose evaluation is described later on). Due to the higher inlet temperatures caused by gas compression, the authors applied the reduction of the engine volumetric compression ratio ρ typically adopted in turbocharged or supercharged engines to avoid knocking. The reduction applied was based on literature data and considerations and the strategies adopted in modern SI engines. With 11 as the CR of the naturally aspirated engine, and assuming a maximum manifold pressure of 1.5 bar, the CR of the turbocharged engine (ρ') was plausibly assumed to be 10, which is in line with current turbocharged VVT engines.

The volumetric efficiency $\lambda_{V,C}$ of the turbocharged engine was evaluated starting from the volumetric efficiency of the naturally aspirated engine λ_{V0} at the same mean piston speed u_m and adjusted using two different corrections. The first one accounted for the pressure difference variation between the inlet and exhaust. The second one was related to the inlet temperature increase (which is well known to cause a volumetric efficiency increase) due to compression. The first correction is given as

$$\frac{\lambda_V'(n)}{\lambda_V(n)} = 1 + \frac{\text{MAP} - p_s}{k \cdot \text{MAP} \cdot (\rho - 1)} \qquad (15)$$

which is 1 if the pressure difference between inlet and exhaust is null. Considering p_{s0} as the reference exhaust backpressure of the baseline naturally aspirated engine, and taking into account the inlet to exhaust pressure difference variation due to the variation of both MAP and p_s, the authors considered, for each mean piston speed, the following correction factor:

$$\frac{\lambda_V(u_m)}{\lambda_{V0}(u_m)} = \frac{1 + \dfrac{\text{MAP} - p_s}{k \cdot \text{MAP} \cdot (\rho - 1)}}{1 + \dfrac{p_0 - p_{s0}}{k \cdot p_0 \cdot (\rho - 1)}} \qquad (16)$$

where λ_{V0} is the baseline naturally aspirated engine volumetric efficiency, corresponding to the manifold pressure p_0 and the exhaust pressure p_{s0} (here assumed = 1.06 p_0). As for the second correction on the volumetric efficiency, i.e., due to the increased inlet temperature, the authors followed the widely adopted relation

$$\frac{\lambda_V(u_m)}{\lambda_{V0}(u_m)} = \sqrt{\frac{T_C}{T_0}} \qquad (17)$$

As a final result, the volumetric efficiency $\lambda_{V,C}$ of the turbocharged engine was evaluated as

$$\lambda_{V,C}(u_m) = \lambda_{V0}(u_m) \cdot \sqrt{\frac{T_C}{T_0}} \cdot \left[\frac{1 + \dfrac{\text{MAP} - p_s}{k \cdot \text{MAP} \cdot (\rho' - 1)}}{1 + \dfrac{p_0 - p_{s0}}{k \cdot p_0 \cdot (\rho - 1)}} \right] \qquad (18)$$

The power balance between turbocompressor and turbine can be resumed as

$$P_{\text{comp}} = P_{\text{turb}} \qquad (19)$$

where P_{comp} is the power required by the turbocompressor

$$P_{\text{comp}} = G_C \cdot \text{cp}_c \cdot \frac{T_0}{\eta_c} \cdot \left(\beta_c^{\frac{k_c-1}{k_c}} - 1 \right) \qquad (20)$$

and P_{turb} is the power delivered by the turbine

$$P_{\text{turb}} = G_T \cdot \text{cp}_s \cdot \eta_t \cdot T_S \cdot \left(1 - \beta_S^{\frac{1-k_s}{k_s}} \right) \qquad (21)$$

where G_C and G_T are the gas mass flow in the compressor and the turbine, respectively, T_0 and T_s are the gas temperatures at compressor and turbine inlet, η_t is the turbine efficiency (whose evaluation is described further on), cp_c and cp_s are the specific heats at a constant pressure of fresh air and exhaust gas, respectively, and $\beta_S = p_s/p_{s0}$ is the pressure ratio across the turbine, with p_s being the gas pressure in the exhaust manifold of the engine. A relation exists between the turbine mass flow G_T and the compressor mass flow G_C

$$G_T = \Omega \cdot G_C \frac{\alpha + 1}{\alpha} \qquad (22)$$

where the ratio $[(\alpha + 1)/\alpha]$ accounts for the fuel mass flow, while Ω represents the fraction of exhaust gas flowing in the turbine, with the rest bypassed by the waste-gate valve if the boosting pressure p_c tends to exceed the maximum allowed value (usually is $0.4 \leq \Omega \leq 1$). The turbocharging compression ratio β_C can be evaluated through the power balance of Eq. (19)

$$\beta_C = \left[1 + \Omega \cdot \frac{\alpha + 1}{\alpha} \cdot \frac{\text{cp}_S}{\text{cp}_C} \cdot \frac{T_S}{T_0} \cdot \eta_T \cdot \eta_C \cdot \left(1 - \frac{1}{\beta_S^{\frac{k_s-1}{k_s}}} \right) \right]^{\frac{k_c}{k_c-1}} \qquad (23)$$

In the calculation performed, the parameter Ω was adaptively reduced (which corresponds to increasing the waste-gate opening) with the aim to prohibit the compression ratio β_C exceeding the maximum allowed value of 1.5. The temperature of the exhaust gas at pressure p_s was evaluated employing a simple yet effective commonly used correlation

$$T_S = T_{1,C} \cdot \frac{p_S}{\text{MAP}} \cdot \frac{(k_S - 1)}{k_S} + \frac{T_{4,C}}{T_{1,C}} \cdot \frac{1}{k_S} \qquad (24)$$

where k_s is the isentropic coefficient of the exhaust gas, $T_{1,C}$ is the inlet temperature at IVC, here assumed equal to the gas temperature at the intercooler outlet T_C, while $T_{4,C}$ is the gas temperature inside the cylinder when the exhaust valves open (EVO). The ratio $T_{4,c}/T_{1,c}$ plays an important role in determining the exhaust gas temperature from Eq. (24). It depends on the physical characteristics of the particular engine and usually varies with changing engine speed and load. For gasoline fueled SI engines, it ranges between 3.5 and 4.5. Given the simple approach followed by the authors in this paper, in the calculation performed, the temperature ratio $T_{4,c}/T_{1,c}$ was supposed to remain constant, apart from engine speed and load variation. However, with the aim to ascertain the importance of its role, the calculations were repeated for three different values of $T_{4,C}/T_{1,C}$, namely, 3.5, 4.0, and 4.5.

The isentropic coefficient k_S in Eq. (24) was computed as

$$k_s = \frac{c_{p,s}(T_s)}{c_{v,s}(T_s)} \quad c_{v,s}(T_s) = c_{p,s}(T_s) - R'_s \qquad (25)$$

where $c_{p,s}$ and $c_{v,s}$ are the burned gas specific heats at constant pressure and constant volume, respectively, both evaluated at the exhaust gas temperature T_s, while R'_s represents the perfect gas law constant. Both $c_{p,s}$ and R'_s were calculated as weighted averages based on the burned gas composition, i.e.,

$$c_{p,s} = c_{p,CO_2}(T_s) \cdot x_{CO_2} + c_{p,H_2O}(T_s) \cdot x_{H_2O} + c_{p,N_2}(T_s) \cdot x_{N_2}$$
$$+ c_{p,CO}(T_s) \cdot x_{CO} \qquad (26)$$

$$R'_s = R'_{CO_2} \cdot x_{CO_2} + R'_{H_2O} \cdot x_{H_2O} + R'_{N_2} \cdot x_{N_2} + R'_{CO} \cdot x_{CO} \qquad (27)$$

where x is the mass fraction of the generic chemical species. For that purpose, to remain as close as possible to gasoline use, the combustion of a surrogate hydrocarbon with $H/C = 1.87$ was considered for the calculation of each mass concentration [22]. The last terms of both Eqs. (26) and (27) refer to the presence of carbon monoxide, which was taken into consideration only when rich air–fuel mixtures were supposed to be employed. For each chemical species, specific heat at constant pressure was computed as a function of the exhaust gas temperature T_s using the Shomate equations and coefficients available on the Chemistry WebBook of the National Institute of Standard and Technology [23].

The system of equations describing the turbocharger power and mass flow balances is completed by the characteristic turbine curve, which correlates the mass flow to the pressure drop and takes into account the turbine swallowing capacity. Following a simplifying approach, a single curve was adopted to describe the mass flow parameter (MFP) of the turbine in place of several curves at different rotation speeds. A suitable mathematical expression was found to faithfully reproduce the typical trend of the MFP as a function of the pressure ratio β_S

$$\text{MFP} = \frac{a \cdot b + c \cdot \beta_S^d}{b + \beta_S^d} \qquad (28)$$

where the model parameters a, b, c, and d were established employing data fitting performed on the characteristics of a real commercial product (IHI-RHF3). Since the turbine mass flow G_T depends on the MFP and the pressure and temperature conditions at the turbine inlet

$$G_T = \text{MFP} \frac{p_S}{\sqrt{T_S}} \qquad (29)$$

the MFP values obtained by Eq. (28) were reduced or amplified, thus sizing the turbine to the engine displacement and the
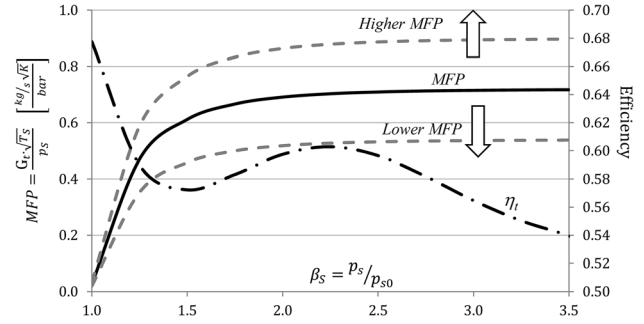
Fig. 9 Performance characteristics of the exhaust gas turbine (efficiency and mass flow parameter as a function of pressure ratio)

parameters resulting from calculations. For example, in Fig. 9, the turbine MFP is represented as a function of the pressure ratio β_S, by a solid curve, while an amplified and a reduced MFP are reported as dashed curves.

A least-square regression, performed on the data available for the already mentioned commercial turbine, allowed determination of a polynomial curve expressing the efficiency as a function of the pressure ratio β_S with a maximum error of 9%

$$\eta_T = -\frac{292.1}{10^4} \beta_S^5 + \frac{3933}{10^4} \beta_S^4 - 2.049\beta_S^3 + 5.113\beta_S^2 - 6.072\beta_S$$
$$+ 3.321 \qquad (30)$$

The resulting efficiency (η_t) curve is also reported in Fig. 9 as a dashed–dotted curve. It is worth highlighting that the efficiency represented in Fig. 9 already accounts for the bearing frictional losses, as indicated by the producer of the commercial turbine. Also, in the case of the turbocompressor, the authors performed an iterative sizing procedure based on the performance map of a commercial unit (IHI-RHF3). To fit a turbocompressor to the engine (whose displacement varies during the whole calculation process), the minimum and maximum values on both axes of the performance map (Fig. 10) were altered with a double task: (1) maintain the operative turbocharging points (expressed by the two coordinates mass flow G_C and compression ratio β_C) within the
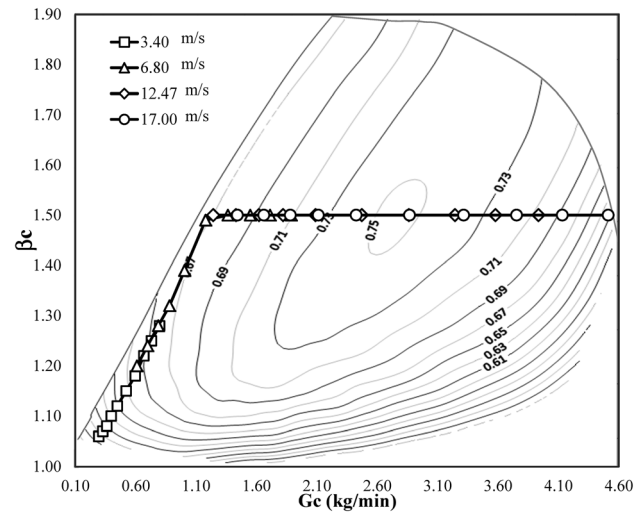
Fig. 10 Turbocharger performance map with reported operative points obtained for every engine load and four different mean piston speeds

Engine		Four-stroke, spark ignition	
Injection system		Gasoline multipoint injection	
Valvetrain		Four valves/cylinder, VVT	
Compression ratio		10	
Maximum boost pressure		1.5 bar	
$T_{4,C}/T_{1,C}$	3.5	4.0	4.5
Displacement	1058 cc	1006 cc	968 cc
Number of cylinders	3	3	3
Bore	74.0 mm	72.7 mm	71.8 mm
Stroke	82.1 mm	80.7 mm	79.7 mm
Maximum BMEP	17.62 bar at 3728 rpm	17.88 bar at 3790 rpm	18.09 bar at 3840 rpm
Minimum BSFC	232.0 g/kWh	230.2 g/kWh	228.9 g/kWh

limits of the contour map, and (2) exploit the best compressor efficiency.

As a result, Fig. 10 shows the turbocharging points required by the engine at four different mean piston speeds. The compressor efficiency (η_C) was deduced from the points' position on the previously digitized contour map. This iterative adaptation of both turbocharger elements represents the selection process usually followed to adequately fit the right turbocharger to the particular engine. Solving the system of equations recursively from Eqs. (13) to (30) for each mean piston speed u_m (from 2.27 to 17 m/s) and manifold pressure MAP (from 0.6 bar up to the maximum allowed value of 1.5 bar) allows calculating the turbocharger performance.

Once the solution for the turbocharger is obtained, the thermodynamic condition of the gas at the engine inlet and outlet can be calculated, which in turn allows evaluating the engine performance. To this purpose, the authors made the simplifying assumption that two similar engines, with the same technology level, running at the same mean piston speed and in full load condition, are characterized by the same gross indicated efficiency, even with different manifold absolute pressures. On account of this assumption, the gross indicated efficiency of the turbocharged engine $\eta_{i,g,c}$ was evaluated based on the gross indicated efficiency of the naturally aspirated engine $\eta_{i,g}$ for the same normalized MAP value and same mean piston speed, and finally corrected to account for the different engine compression ratio. Defining the normalized MAP as

$$\phi = \frac{\text{MAP}}{\text{MAP}_{\text{max}}} \tag{31}$$

the simplifying assumption gives

$$\eta_{i,g,C}(\phi, u_m) = \eta_{i,g}(\phi, u_m) \cdot f_{\text{CR}} \tag{32}$$

where f_{CR} is the correction factor used to account for the different CR between turbocharged and naturally aspirated engines, calculated through the basic theory of the ideal Otto cycle

$$f_{\text{CR}} = \frac{\eta'_{\text{Otto}}}{\eta_{\text{Otto}}} = \frac{1 - \dfrac{1}{\rho'^{k-1}}}{1 - \dfrac{1}{\rho^{k-1}}} \tag{33}$$

The gross indicated mean effective pressure of the turbocharged engine was hence evaluated as

$$\text{IMEP}_{g,C} = \frac{\delta_C \cdot \lambda_{V,C} \cdot \text{LHV}}{\alpha + \frac{1}{\delta'}} \cdot \eta_{i,g,C} \tag{34}$$

and the resulting net indicated mean effective pressure as

$$\text{IMEP}_C = \text{IMEP}_{g,C} + \text{PMEP}_C \tag{35}$$

where the pumping mean effective pressure PMEP_C was simply evaluated as

$$\text{PMEP}_C = \text{MAP} - p_s \tag{36}$$

The friction mean effective pressure was computed employing the same Eq. (3) used for the naturally aspirated engine; the turbocharged engine brake mean effective pressure BMEP_C could be hence calculated together with the related brake specific fuel consumption BSFC_C

$$\text{BMEP}_C = \text{IMEP}_C + \text{FMEP}_C \tag{37}$$

$$\text{BSFC}_C = \frac{\delta_C \cdot \lambda_{V,C}}{\text{BMEP}_C \cdot \left(\alpha + \frac{1}{\delta'}\right)} \tag{38}$$

The maximum BMEP_C calculated for the turbocharged engine was used to determine the displacement V_T necessary to deliver the required output power of 73.5 kW. As mentioned before, the entire calculation was repeated considering the three different values of the temperature ratio $T_{4,C}/T_{1,C}$. The main characteristics and performance of the resulting reference turbocharged engine are summarized in Table 3, while Fig. 11 reports the brake specific fuel consumption contour map obtained for the reference turbocharged engine with $T_{4,C}/T_{1,C} = 4$.
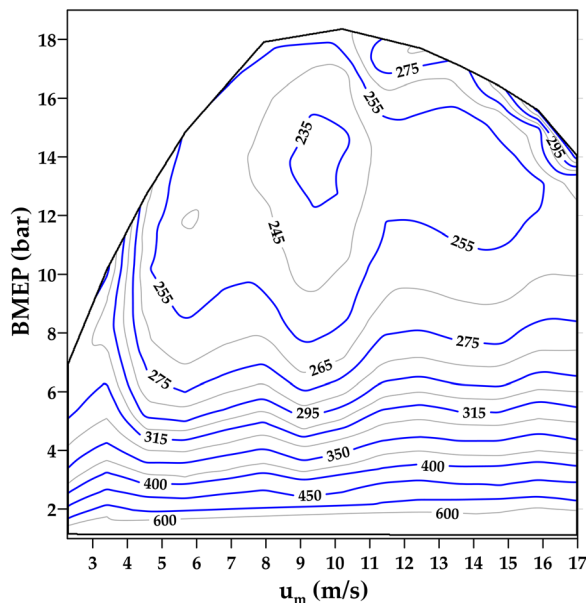

Fig. 11 Brake specific fuel consumption (g/kWh) of the turbocharged engine ($T_{4,C}/T_C = 4$)
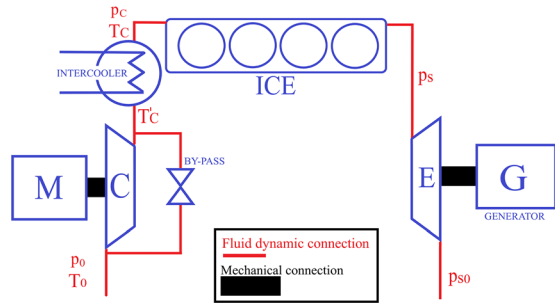
Fig. 12 Schematic representation of the separated electric compound engine (C = compressor; E = expander; ICE = internal combustion engine; M = electric motor; and G = electric generator)

Separated Electric Compound Spark-Ignition Engine

This section presents the procedure followed to evaluate the performance of the proposed CE and the resulting comparison with the traditional reference turbocharged engine carried out in a hybrid propulsion architecture. Figure 12 provides a schematic representation of the compound system, composed of a SI engine, an electric driven supercharger, and an expander–generator group to complete the exhaust gas expansion. Unlike the traditional turbocharged engine, the compressor is not connected to the expander but is driven by the electric motor, which, in turn, is powered by the same energy storage system (e.g., the batteries of the hybrid vehicle) which receives the power produced by the expander–generator. Furthermore, the management system is assumed to control the rotation speed of the motor–compressor to increase the air pressure only when needed (i.e., when MAP values higher than 1 bar are required) and reduce its power absorption for the part-load operation (i.e., when MAP < 1 bar). As illustrated in Fig. 12, a bypass valve lets the air flow to the engine in this condition.

The expander–generator group is considered permanently active, thus continuously recovering the maximum possible power from the exhaust gas. Regarding the compressor, a turbocompressor similar to the one considered for the turbocharged engine was employed. Hence, its efficiency was evaluated following the same calculation (and sizing) procedure described in the section Reference Turbocharged Engine. However, other opportunities may be considered, such as using a Roots-type or a screw compressor, which are commonly employed for engine supercharging. Regarding the exhaust gas expander represented in Fig. 12, it must be pointed out that such a machine is not currently available on the market. This machine is substantially different from turbines commonly used for turbocharging purposes. These turbines, in effect, consist of a single radial stage designed to deliver sufficient power to drive the turbocompressor. They usually function under wide variations of speed and mass flow and as a result are not optimized for steady-state operation.

In contrast to a conventional powertrain, the exhaust gas expander to be employed in the CE considered here is involved in hybrid propulsion application and should function under almost steady-state conditions. Moreover, the generator's torque/current control would let the expander run at its best efficiency speed ratio, independently from the power produced. As a result, the exhaust gas expander considered in this work should be composed of two or more stages, optimized for power production, and deliver power up to 16 kW (as shown further on) with efficiency higher than common turbocharging turbines. The only products already available on the market, or studied up to now, [24–26], consist of radial turbines derived from turbocharging, connected to electric generators, and characterized by limited power (6 kW), being designed only to supply the vehicle electric accessories. According to the previous considerations, the authors reasoned that, apart from the power produced, the exhaust gas expander should work with almost unchanged speed ratio and, hence, with

constant efficiency η_E. With the aim to ascertain the effect of the expander efficiency on the overall energetic performance of the CE, two different efficiency levels were considered, 0.70 and 0.75. As already explained, the two assumed efficiency values are significantly higher than in a common turbocharging turbine under the assumption that the exhaust gas expander should be a machine conceived and optimized for steady-state power production.

The performance of the CE concept was evaluated at the same mean piston speed u_m (from 2.27 to 17 m/s) and MAP values (from 0.6 bar to the maximum allowed 1.5 bar) as the turbocharged engine. The inlet air density δ_C was evaluated using Eqs. (11), (13), and (14). The gross indicated mean effective pressure of the supercharged engine is given as

$$\text{IMEP}_{g,C} = \frac{\delta_C \cdot \lambda_{V,C} \cdot \text{LHV}}{\alpha + \frac{1}{\delta'}} \cdot \eta_{i,g,C} \qquad (39)$$

The $\text{IMEP}_{g,C}$ was then evaluated after determining both indicated gross efficiency $\eta_{i,g,c}$ and volumetric efficiency $\lambda_{V,C}$.

It can be observed that the use of the exhaust gas expander produces an increase in the exhaust gas back pressure p_s. The effect is stronger than in a common turbocharged engine for at least two reasons. First of all, the expander–generator group is always active, even at partial load operation, when the engine manifold absolute pressure is lower than 1 bar. Second, unlike the turbocharged system, where part of the exhaust mass flow bypasses the turbine through the waste-gate valve, in the system proposed, the task of the expander is to exploit the maximum available power, working with the whole exhaust mass flow and with sufficiently high-pressure ratio $\beta_S = p_s/p_{s0}$.

It is evident that changing the exhaust backpressure may have repercussions on both the volumetric efficiency and the indicated efficiency of the engine. Increasing the exhaust pressure causes a small increase in the amount of in-cylinder residual gas, resulting in a reduction of the entrapped fresh charge and, hence, reduced engine volumetric efficiency. Moreover, with the flame propagation speed and combustion efficiency strongly influenced by fresh charge dilution with residual gas, an exhaust pressure increase could easily compromise engine indicated efficiency. Based on these considerations, the effect produced by the exhaust pressure increase was carefully considered. Regarding the volumetric efficiency, Eq. (18) was used to account for the pressure difference effect between the intake and the exhaust. Concerning the second effect, i.e., the indicated efficiency worsening due to the exhaust pressure increase, no useful reference could be found in the scientific literature.

To compensate for lack of available literature on the effect of exhaust back pressure, the authors executed a dedicated series of experimental tests on a SI engine test bench, with the aim to correlate the in-cylinder residual gas fraction (RGF) increment to the indicated efficiency deterioration. For that purpose, a throttle valve was installed in the exhaust duct of a four-cylinder multipoint 1.2 L SI engine and used to modulate the exhaust backpressure. In-cylinder pressure was measured using an AVL GU13X piezoelectric pressure sensor flush-mounted in the combustion chamber and sampled with the resolution of 1 crank angle degree, together with air and fuel mass flows, manifold absolute pressure, and engine torque. A more detailed description of the engine test bed employed is reported in Refs. [27] and [28].

Table 4 summarizes the operating conditions of the experiment expressly performed to determine the relationship between the exhaust pressure increase and the indicated efficiency deterioration. For each tested engine speed, a 0.1 bar increment of exhaust pressure was imposed until heavy combustion instability was found up to a maximum of 2 bar. The tests were performed employing compressed natural gas as fuel in place of gasoline. It was assumed that the particular fuel employed had a negligible influence on the relation between indicated efficiency variation and exhaust pressure variation.

Table 4 Operating conditions of the experimental test

Engine speed (rpm)	1500–2500–3500
Engine load	Full
MAP (bar)	1.00
Exhaust pressure p_s (bar)	1.0 to 2.0 in steps of 0.1
Fuel	Compressed natural gas
Spark advance	Optimized setting the location of peak pressure to 15 crank angle degree after top dead centre
Air–fuel ratio	Stoichiometric

As shown in Fig. 13, the results of the tests performed confirmed that an exhaust pressure increase (with constant MAP) reduces the gross indicated thermal efficiency of the engine due to the increased residual gas fraction (i.e., the ratio between the residual gas mass and the total in-cylinder mass). The experimental measurements revealed that the variation of the gross indicated efficiency can be expressed as a function of the residual gas fraction increment using the relation

$$\frac{\eta_{i,g,C}}{\eta_{i,g,C,0}} = \frac{1}{1 + b \cdot x^\gamma}$$

$$b = 0.1384 \cdot u_m^{-2.635} \quad \gamma = -0.2556 \cdot u_m + 6.0391 \tag{40}$$

where $\eta_{i,g,C,0}$ is the reference gross indicated efficiency of the engine (i.e., without throttling the exhaust duct), $x = \text{RGF}/\text{RGF}_0$ is the ratio between the RGF measured with and without exhaust throttling (whose evaluation is described in the Appendix), while the parameters b and γ are correlated to the mean piston speed u_m, which, as shown in Fig. 13, has a strong influence on the efficiency variation.

The performance of the supercharged engine was evaluated compared to the baseline engine according to the mentioned assumption that the same technology level produces equal specific performances unless modification or parameters variations occur. The gross reference indicated that the efficiency $\eta_{i,g,C,0}$ of the engine (i.e., without throttling the exhaust duct) was evaluated according to the same assumption made for the turbocharged reference engine, i.e., using Eqs. (31)–(33), where the engine CR was considered reduced to 10 also in this case

$$\eta_{i,g,C,0}(\phi, u_m) = \eta_{i,g}(\phi, u_m) \cdot f_{CR} \tag{41}$$

The gross indicated efficiency $\eta_{i,g,c}$ of the supercharged engine was hence calculated by means of Eqs. (40) and (41) for each MAP and mean piston speed. Hence, the net indicated mean effective pressure IMEP_C could be computed as

$$\text{IMEP}_C = \text{IMEP}_{g,C} + \text{PMEP}_C \tag{42}$$

where the pumping mean effective pressure PMEP_C was obtained by Eq. (36). Equations (3) and (37) were then employed to evaluate the FMEP_C and the engine BMEP_C, respectively.
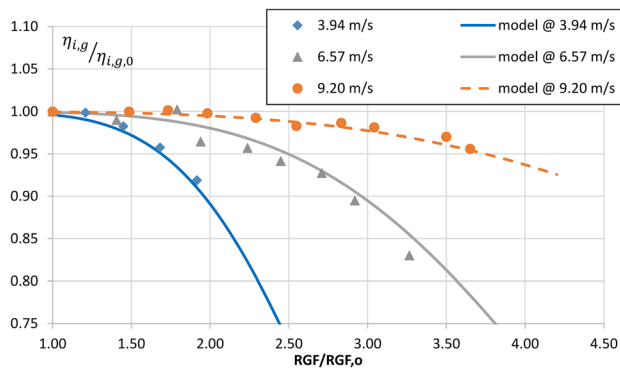
Fig. 13 Gross IMEP variation as a function of the RGF increment

The overall specific output of the compound system BMEP_{TOT} is composed by the engine BMEP_C, with the addition of the specific output of the expander–generator group (here called recovery mean equivalent pressure RMEP), and the reduction due to the specific power required by the motor–compressor (here called compressor mean equivalent pressure CMEP)

$$\text{BMEP}_{tot} = \text{BMEP}_C + \text{RMEP} - \text{CMEP} \tag{43}$$

The recovery mean effective pressure is clearly related to the power recovered by the expander P_{exp}

$$\text{RMEP} = \frac{60 \cdot \varepsilon \cdot P_{exp}}{V_C \cdot n} \tag{44}$$

where ε is the number of revolutions per cycle (2 for a four-stroke engine), and V_C is the supercharged engine displacement. Similarly, the compressor mean effective pressure is related to the power required by the compressor P_{comp}

$$\text{CMEP} = \frac{60 \cdot \varepsilon \cdot P_{comp}}{V_C \cdot n \cdot \eta_{EM}} \tag{45}$$

where η_{EM} is the electric motor efficiency, considered here since the motor–compressor represents an ancillary device that burdens the engine's energy balance. According to Eq. (44), the generator's efficiency was not considered in the RMEP calculation coherently with the evaluation of the power produced by the engine, which was not reduced by the efficiency of the electrical machine connected in the generic hybrid propulsion system. The power required by the compressor has the same formulation given in Eq. (20), while, similarly to the power delivered by the turbine of Eq. (21), the power produced by the expander P_{exp} can be expressed as

$$P_{exp} = G_C \cdot \frac{\alpha + 1}{\alpha} \cdot \text{cp}_s \cdot \eta_E \cdot T_S \cdot \left(1 - \beta_S^{\frac{1-k_s}{k_s}}\right) \tag{46}$$

where T_S is the exhaust gas temperature at the expander inlet (evaluated using Eq. (24)), α is the air–fuel ratio, G_C is the air mass flow to the engine, η_E is the expander efficiency, $\beta_S = p_s/p_{s0}$ is the pressure ratio across the expander, k_S and cp_s are the isentropic coefficients and the constant pressure specific heat of the exhaust gas, both evaluated at the temperature T_S, as already described through Eqs. (25)–(27). Given the air mass flow to the engine

$$G_C = \frac{V_T \cdot n}{60 \cdot \varepsilon} \cdot \delta_C \cdot \lambda_{V,C} \frac{\alpha}{\alpha + \frac{1}{\delta'}} \tag{47}$$

Recovery mean equivalent pressure and CMEP become:

$$\text{RMEP} = \delta_C \cdot \lambda_{V,C} \cdot \frac{\alpha + 1}{\alpha} \cdot c_{p,s} \cdot T_s \cdot \eta_E \cdot \left(1 - \beta_S^{\frac{1-k_s}{k_s}}\right) \tag{48}$$

$$\text{CMEP} = \frac{\delta_C \cdot \lambda_{V,C} \cdot \text{cp}_c \cdot T_0}{\eta_{EM} \cdot \eta_C} \cdot \left(\beta_c^{\frac{k_c-1}{k_c}} - 1\right) \tag{49}$$

For each mean piston speed u_m and manifold absolute pressure MAP, the overall brake thermal efficiency $\eta_{b,TOT}$ of the proposed compound system is

$$\eta_{b,TOT} = \frac{\text{BMEP}_{TOT} \cdot \left(\alpha + \frac{1}{\delta'}\right)}{\delta_C \cdot \lambda_{V,C} \cdot \text{LHV}}$$

$$= \frac{(\text{BMEP} + \text{RMEP} - \text{CMEP}) \cdot \left(\alpha + \frac{1}{\delta'}\right)}{\delta_C \cdot \lambda_{V,C} \cdot \text{LHV}} \tag{50}$$

It is worth noting that, for each required output power, or, which is the same, for each BMEP$_{TOT}$, the overall efficiency of the considered compound system depends on the exhaust pressure; on the one hand, boosting the exhaust pressure produces higher RMEP, on the other hand, it causes PMEP increments (Eq. (36)) and indicates efficiency reduction (Eq. (40)) due to the increased amount of residual gas mass, and, as a final result, a decrease of engine BMEP. Therefore, for each power level (or BMEP$_{TOT}$), a compromise exists between the advantages and disadvantages produced by the exhaust pressure increase. The optimal exhaust pressure value was determined to be the value corresponding to the maximum overall brake thermal efficiency $\eta_{b,TOT}$ for each engine load (MAP) and speed (u_m). A genetic algorithm was employed for the optimization process, since $\eta_{b,TOT}$ is not a linear or polynomial function of the exhaust pressure. This procedure was repeated for each considered temperature ratio $T_{4,C}/T_{1,C}$ (3.5, 4.0, and 4.5) and for each expander efficiency η_E (0.70 and 0.75). For example, Figs. 14 and 15 report the contour maps of the optimal exhaust pressure levels determined for each overall load and mean piston speed for the two extreme cases $T_{4,C}/T_{1,C} = 3.5$—$\eta_E = 0.70$ and $T_{4,C}/T_{1,C} = 4.5$—$\eta_E = 0.75$.

It can be noted that, for the higher power level, the optimal exhaust pressure was estimated to range between 2.6 and 3.3 bar: this requirement should be adequately considered in the optimal design of the exhaust gas expander. It was also observed that the optimal exhaust pressure increased when considering higher temperature ratio $T_{4,C}/T_{1,C}$ or higher expander efficiency η_E.

The overall brake specific fuel consumption of the compound engine BSFC$_{TOT}$ was evaluated from the overall brake mean effective pressure

$$\text{BSFC}_{TOT} = \frac{\delta_C \cdot \lambda_{V,C}}{\text{BMEP}_{TOT} \cdot \left(\alpha + \frac{1}{\delta'}\right)} \quad (51)$$

Figure 16 represents the contour map of the specific fuel consumption obtained for the case $T_{4,C}/T_{1,C} = 4$ and $\eta_E = 0.7$, which can be compared to the map traced for the reference turbocharged engine with the same temperature ratio $T_{4,C}/T_{1,C}$ (shown in Fig. 11). It can be observed that the proposed compound system exhibits better fuel economy even though the two propulsive solutions obtained similar BMEP. Once the optimal exhaust pressure levels were determined, the maximum value of the BMEP$_{TOT}$ allowed determining the engine displacement V_C necessary to develop the target power of 73.5 kW. Table 5 summarizes the main characteristics of the CE together with some performance
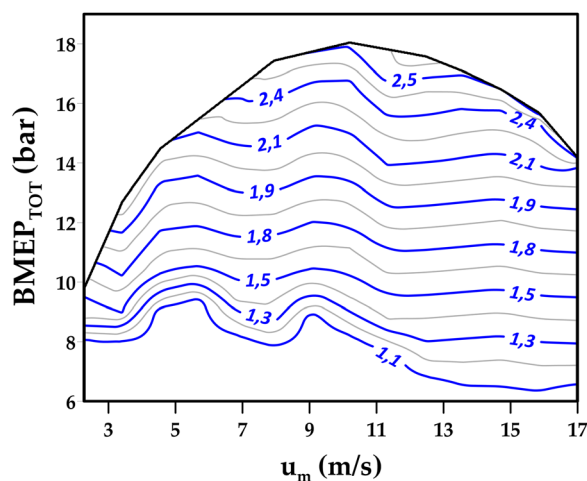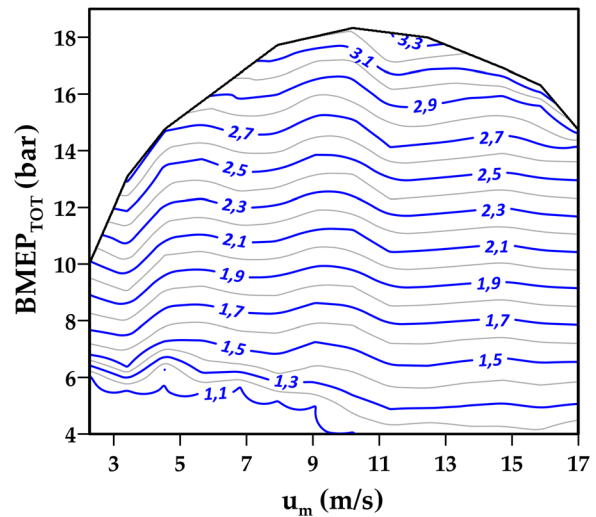

Fig. 15 Optimal exhaust pressure levels as a function of load and speed ($\eta_E = 0.75$ and $T_{4,c}/T_{1,c} = 4.5$)

parameters for each value adopted for the temperature ratio $T_{4,C}/T_{1,C}$ and considering the expander efficiency of 0.70.

In comparison, Table 6 summarizes the results obtained considering an expander efficiency of 0.75.

The compound system considered here revealed approximately the same specific output power (BMEP$_{TOT}$) as the reference turbocharged engine (reported in Table 3). Regarding fuel economy, apart from the expander efficiency and the temperature ratio, the minimum fuel consumption obtainable by the electric CE is always lower than the consumption of the turbocharged reference engine. Reductions between 5.1% and 8.3% have been found. Tables 5 and 6 also report the maximum value assumed by the RMEP, which ranged from 2.90 to 4.62 bar (corresponding to the power delivered between 10.8 and 16.6 kW), and revealed a higher sensitivity to the temperature ratio (with increments up to 43%) than to the expander efficiency (increments of about 12%). The same tables also show that the expander contributes to the overall output power, with a maximum share of power contribution from 19% to 33%, depending on the particular temperature ratio or expander efficiency. This means that, if adequately

Fig. 14 Optimal exhaust pressure levels as a function of load and speed ($\eta_E = 0.7$ and $T_{4,c}/T_{1,c} = 3.5$)
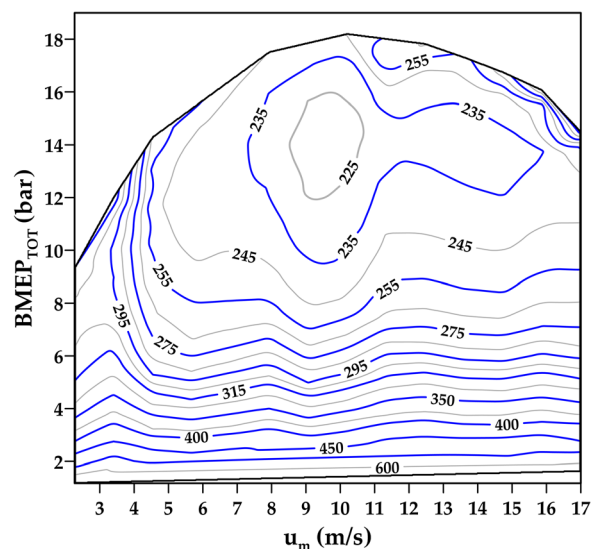

Fig. 16 Brake specific fuel consumption (g/kWh) of the CE, as a function of overall load and mean piston speed ($T_{4,c}/T_{1,c} = 4$ and $\eta_E = 0.7$)

Table 5　Main characteristic of the CE obtained with $\eta_E = 0.70$

Engine	Four-stroke, spark ignition		
Injection system		Gasoline multipoint injection	
Valvetrain		Four valves/cylinder, VVT	
Compression ratio		10	
Maximum boost pressure		1.5 bar	
Expander efficiency		0.7	
$T_{4,C}/T_{1,C}$	3.5	4.0	4.5
Displacement	950 cc	923 cc	905 cc
Number of cylinders	3	3	3
Bore	71.3 mm	70.7 mm	70.2 mm
Stroke	79.2 mm	78.4 mm	77.9 mm
Maximum $BMEP_{TOT}$	17.83 bar at 3864 rpm	17.90 bar at 3900 rpm	18.00 bar at 3926 rpm
Minimum $BSFC_{TOT}$	220.2 g/kWh	216.6 g/kWh	212.7 g/kWh
Variation of minimum BSFC	−5.1%	−5.9%	−7.1%
Maximum RMEP	2.90 bar at 4722 rpm	3.52 bar at 4768 rpm	4.16 bar at 4799 rpm
Maximum $RMEP/BMEP_{TOT}$	19%	23.9%	29.2%

Table 6　Main characteristic of the CE obtained with $\eta_E = 0.75$

Engine	Four-stroke, spark ignition		
Injection system		Gasoline multipoint injection	
Valvetrain		Four valves/cylinder, VVT	
Compression ratio		10	
Maximum boost pressure		1.5 bar	
Expander efficiency		0.75	
$T_{4,C}/T_{1,C}$	3.5	4.0	4.5
Displacement	938 cc	912 cc	896 cc
Number of cylinders	3	3	3
Bore	71.0 mm	70.4 mm	70.0 mm
Stroke	78.9 mm	78.1 mm	77.7 mm
Maximum $BMEP_{TOT}$	17.85 bar at 3880 rpm	18.00 bar at 3917 rpm	18.10 bar at 3939 rpm
Min $BSFC_{TOT}$	218.3 g/kWh	214.3 g/kWh	210.0 g/kWh
Variation of min BSFC	−5.9%	−6.9%	−8.3%
Max RMEP	3.27 bar at 4743 rpm	3.94 bar at 4788 rpm	4.62 bar at 4815 rpm
Max $RMEP/BMEP_{TOT}$	21.9%	27.4%	33.3%

recovered, the unexpanded gas energy may constitute a relevant part of the whole propulsion energy and may contribute to lowering both the vehicle fuel consumption and related emissions.

Although the initial results are promising, a comparison based on minimum fuel consumption or maximum specific power is not exhaustive. Considering the application to hybrid propulsion vehicle, a comparison between the proposed CE and the traditional turbocharged engine was carried out on an equal output power basis. Figures 17 and 18 show, for the two extreme cases ($T_{4,C}/T_{1,C} = 3.5$, $\eta_E = 0.70$ and $T_{4,C}/T_{1,C} = 4.5$, $\eta_E = 0.75$, respectively), the efficiency improvement obtainable by the proposed CE for the reference turbocharged engine, as a function of the (overall) output power and mean piston speed. The first observation is that the energetic advantage of the expander–generator increases with the overall output power. This observation can be easily explained considering that the power contribution of the expander increases with the exhaust gas mass flow and the in-cylinder pressure levels. In further detail, the efficiency improvement remains within 5% for power level within 10 kW, reaching a maximum of about 10% in the first case (Fig. 17) and 12% in the second (Fig. 18) at the maximum output power. This is an encouraging result, especially because the effect of the increased exhaust pressure on the gross indicated efficiency was not considered for the turbocharged engine.

Moreover, better improvements were obtained with the higher expander efficiency and temperature ratio. Hence, it can be concluded that a proper study and optimization of the compound performance of both engine and expander could allow even better results. To ascertain the effect on an aftertreatment device like a catalyst, whose inlet gas temperature should safely remain above 400 °C, the exhaust gas temperature downstream the expander

was also evaluated. As expected, the worst case is represented by $T_4/T_1 = 3.5$ and expander efficiency $\eta_E = 0.75$, which gave expander outlet temperatures between 808 and 918 K, depending
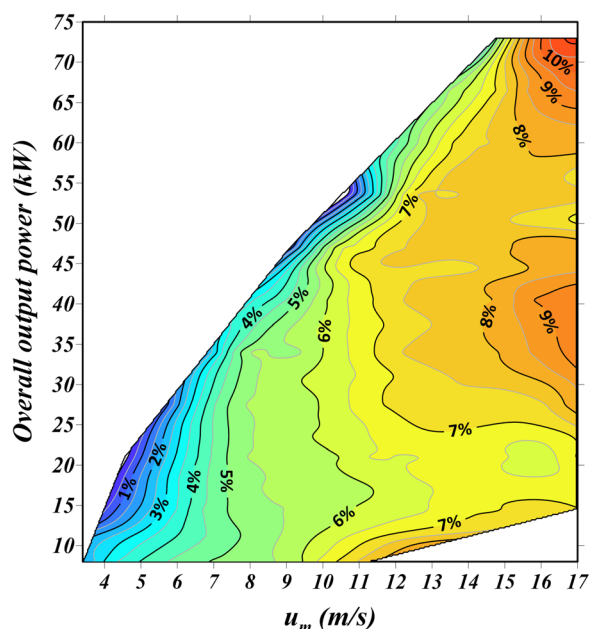

Fig. 17　Efficiency improvement of the CE compared to the reference turbocharged engine as a function of power output and mean piston speed ($T_{4,C}/T_{1,C} = 3.5$ and $\eta_E = 0.70$)
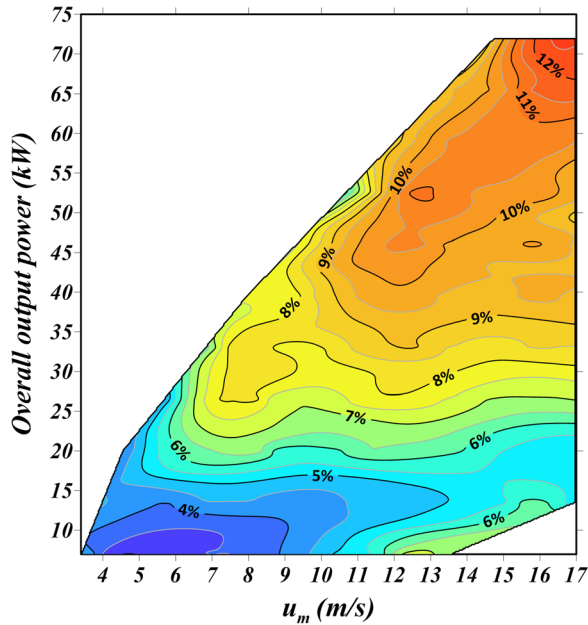
Fig. 18 Efficiency improvement of the CE compared to the reference turbocharged engine as a function of power output and mean piston speed ($T_{4,C}/T_{1,C} = 4.5$ and $\eta_E = 0.75$)

Fig. 20 Comparison between the best efficiencies obtained for different power output ($T_{4,C}/T_{1,C} = 4.5$ and $\eta_E = 0.75$)

on the engine load and speed of rotation. These temperatures are, however, sufficiently higher to allow a stable and efficient conversion in the catalyst. Hence, it may be concluded that the expander–generator implementation would not cause any critical situation for exhaust aftertreatment devices like three-way catalysts.

Focusing on the hybrid propulsion, however, it is worth pointing out that in such vehicles, the thermal machine is usually employed on its best efficiency curve, i.e., the curve connecting the operative conditions which ensure, for each power request, the maximum efficiency. Therefore, a further, and fairer, comparison could be based on the best efficiency curves of both CE and turbocharged engine. To this purpose, for each output power, the authors determined the best efficiency operative conditions (load and speed) on each of the two propulsive solutions. The results of this evaluation are reported in Fig. 19, which refers to the case $T_{4,C}/T_{1,C} = 3.5$ and $\eta_E = 0.70$, and Fig. 20, obtained considering $T_{4,C}/T_{1,C} = 4.5$ and $\eta_E = 0.75$. Both diagrams report the best efficiency curves of the two propulsive solutions, together with the efficiency increments obtainable by the proposed CE system. It should be noted that the benefit introduced by the exhaust energy recovery strictly depends on the output power level (as already revealed by the contour maps in Figs. 17 and 18) and may reach values as high as 8.3% in the first case and 12.8% in the second. Considering the entire power range, the average efficiency
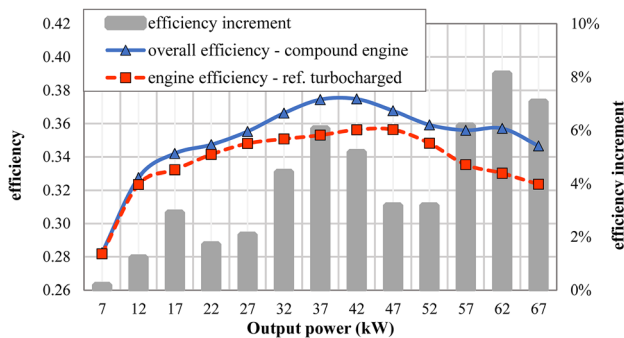

Fig. 19 Comparison between the best efficiencies obtained for different power output ($T_{4,C}/T_{1,C} = 3.5$ and $\eta_E = 0.70$)
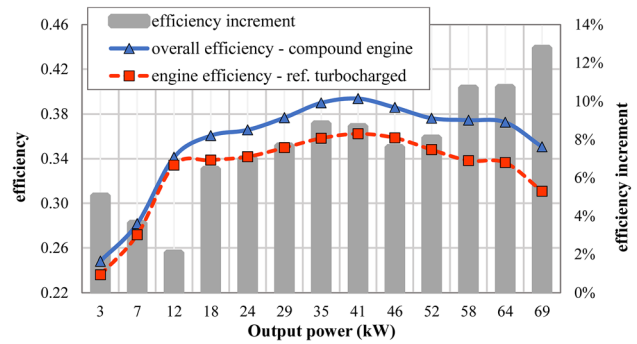
increased by 4.1% compared to the turbocharged engine in Fig. 19 and 7.7% in Fig. 20.

According to the results obtained by this last comparison, the compound system composed of an electrically supercharged SI engine equipped with an exhaust expander–generator has excellent potential to improve fuel economy with corresponding emissions reduction. Hence, it can be concluded that the CE system merits further and deeper investigation, focusing on the optimization of the compound system constituted by the engine and the expander–generator. Research and development should also be carried out on the expander–generator unit itself, as performance strictly influences the energetic advantages of the proposed compound system.

Conclusion

In this paper, the authors evaluated the energetic advantages of a separated electric CE, i.e., a propulsive unit composed of an electrically supercharged SI engine equipped with an exhaust gas expander connected to an electric generator, to transform the unexpanded exhaust gas energy, typical of conventional thermodynamic engine cycles, into electrical energy. The system proposed is specifically intended for hybrid vehicles, where the energy produced by the expander–generator can be stored in the storage system and hence profitably employed for vehicle propulsion.

Several operating conditions were assessed to evaluate the effective applicability of the proposed CE in a vehicle scenario, and the resulting overall efficiency was compared to the efficiency of a reference turbocharged engine. The comparison was carried out considering a hybrid vehicle application, i.e., on an equal output power basis and in steady-state operative conditions. To remain as close as possible to the real engine efficiency, actual engine performance data and values retrieved from literature or experimental tests were adopted in the simple and effective calculations performed.

Moreover, to make the result obtained reliable and valid on a wide range of engines, three different values were considered for the temperature ratio T_4/T_1 (namely, 3.5, 4.0, and 4.5), which is the ratio between the in-cylinder gas temperature at the end of the expansion stroke and the beginning of the compression stroke. This temperature ratio depends on the particular engine configuration and specification. It strongly influences the temperature of the exhaust gas entering the expander or the turbine, thus playing an important role in determining the energetic advantage of the CE proposed concerning the reference turbocharged engine. Also, the exhaust gas expander plays a fundamental role and may substantially affect the entire system's efficiency. For this reason, the effect of a variation of its average efficiency was also taken into account by considering two different efficiency values (namely, 0.70 and 0.75).

When considering the exhaust gas expander, the effect of exhaust backpressure variation on engine efficiency, pumping

cycle, and volumetric efficiency was carefully considered. Hence, the optimal exhaust pressure of the proposed CE was established for each operative condition, maximizing its overall efficiency. As expected, the advantage connected to the exhaust gas energy recovery increased with the overall output power, which has been explained considering that the power contribution of the expander increases with the exhaust gas mass flow and with the in-cylinder pressure levels. As a final result, considering the whole operative condition map, the efficiency improvement obtained by the CE reached a maximum value between 10% and 12%, depending on the particular temperature ratio or expander efficiency considered. Furthermore, focusing on the hybrid vehicle application, the authors restricted the efficiency comparison to the best efficiency curves of each propulsive unit: in this case, the maximum advantage of the CE varied between 8.3% and 12.8%.

The evaluation performed also established that the contribution of the expander–generator to the overall power produced by the CE could be considerable, reaching a share of 33% and a maximum delivered power of 16.6 kW. This means that, if adequately recovered, the unexpanded gas energy may constitute a relevant part of the whole propulsion energy and may contribute to lower both vehicle fuel consumption and related emissions.

Regarding the expander operating conditions, the optimal exhaust gas pressure was estimated to range between 2.6 bar and 3.3 bar. Moreover, better improvements were obtained for the higher speed and load of the engine, meaning that the exhaust gas temperature T_S at the expander inlet could reach $800 - 900\,°C$. These results should be properly considered for an optimized expander design, which could be a multistage radial–axial turbine. Furthermore, as expected, better improvements were obtained with higher expander efficiency and temperature ratio. It can be concluded that a proper study and optimization of the compound performance of both engine and expander could achieve even more significant results than those presented here.

Funding Data

Nomenclature

Symbols/Abbreviations

a, b, c = parameters of the turbine MFP model
BMEP = brake mean effective pressure
BSFC = brake specific fuel consumption
$BMEP_{max}$ = maximum BMEP
$BMEP_{TOT}$ = overall BMEP of the compound engine
$BSFC_{TOT}$ = overall BSFC of the compound engine
$c_{p,c}$ = specific heat at a constant pressure of the air
$c_{p,s}$ = specific heat at a constant pressure of burned gas
$c_{p,u}$ = specific heat at a constant pressure of unburned gas
CE = compound engine
CMEP = compressor mean equivalent pressure
CR = volumetric compression ratio
EVO = exhaust valve open
f_{CR} = correction factor related to compression ratio
FMEP = friction mean effective pressure
G_C = air mass flow (turbo/supercharged engine)
G_O = air mass flow (naturally aspirated engine)
G_T = turbine gas mass flow
IMEP = indicated mean effective pressure
IVC = intake valve closure
$IMEP_g$ = gross indicated mean effective pressure
k_S = isentropic coefficient of the exhaust gas
LHV = lower heating value of the fuel
m_S = residual gas mass
m_0 = fresh charge mass
MAP = manifold absolute pressure

MAP_{max} = maximum MAP
p_c = boosting pressure
P_{comp} = power required by the compressor
P_{exp} = power produced by the expander
p_s = engine exhaust pressure
p_{s0} = exhaust pipe pressure
PMEP = pumping mean effective pressure
R_{INT} = intercooler efficiency
R_S' = specific gas constant of exhaust gas or burned gas
RGF = residual gas fraction
RMEP = recovery mean equivalent pressure
SI = spark ignition
T = temperature
T_C = air temperature at the intercooler outlet
T_R = residual gas temperature
T_S = exhaust gas temperature
T_0 = air temperature in the intake manifold
T_1 = in-cylinder gas temperature at IVC
T_4 = in-cylinder gas temperature at EVO
T_C' = air temperature at the compressor outlet
u = normalized mean piston speed $= u_m/u_{m,max}$
u_m = mean piston speed
$u_{m,max}$ = maximum mean piston speed
V_A = naturally aspirated engine displacement
V_C = engine displacement in the compound unit
V_T = turbocharged engine displacement
α = air–fuel ratio
α_{st} = stoichiometric air–fuel ratio
β_C = compressor pressure ratio
β_S = expander and turbine pressure ratio
γ, σ = parameters of the model for the gross indicated efficiency variation as a function of RGF
δ_C = density of the compressed air in the intake manifold
δ_0 = air density in the intake manifold
ε = number of revolutions per cycle
η_b = brake thermal efficiency of the engine
$\eta_{b,max}$ = maximum brake thermal efficiency of the engine
$\eta_{b,TOT}$ = overall brake thermal efficiency of the compound engine
η_C = compressor efficiency
η_E = expander efficiency
η_{EM} = electric motor efficiency
η_i = indicated thermal efficiency of the engine
$\eta_{i,g}$ = gross indicated thermal efficiency of the engine
$\eta_{i,max}$ = maximum indicated thermal efficiency of the engine
η_m = overall mechanical efficiency of the engine
η_T = turbine efficiency
λ = relative air–fuel ratio
λ_V = volumetric efficiency of the engine
$\lambda_{V,C}$ = volumetric efficiency of supercharged/turbocharged engine
$\lambda_{V,max}$ = maximum volumetric efficiency of the engine
ρ = engine compression ratio (naturally asp.)
ρ' = engine compression ratio (turbo/supercharged)
ϕ = relative MAP $= MAP/MAP_{max}$
ψ = normalized load variable $= BMEP/BMEP_{max}$

Subscripts

c = compression/compressed
g = gross
s = exhaust gas
0 = reference condition

Appendix: Residual Gas Fraction Evaluation

When engine IVC, the mass entrapped in the cylinder results in the sum of the residual gas from the previous cycle (m_S) and of the fresh charge (m_0); the RGF, which represents the ratio between the residual gas mass and the total in-cylinder mass, is hence

$$\text{RGF} = \frac{m_S}{m_{\text{TOT}}} = \frac{m_S}{m_0 + m_S} \tag{A1}$$

The fresh charge mass entrapped in the cylinder depends on the engine volumetric efficiency λ_V

$$m_0 = \lambda_V \cdot \frac{\text{MAP}}{R'_0 \cdot T_0} \cdot V \tag{A2}$$

where T_0 and MAP are the temperature and pressure in the intake manifold, respectively, and V is the engine displacement. Assuming the residual gas mass as the amount of in-cylinder exhaust gas at the ideal end of the exhaust stroke (i.e., at top dead center)

$$m_S = \frac{p_S}{R'_S \cdot T_R} \cdot \left(\frac{V}{\rho - 1} \right) \tag{A3}$$

where T_R and p_s represent the temperature and pressure of the in-cylinder residual gas, ρ is the engine compression ratio, and hence $V/(\rho - 1)$ the in-cylinder volume at top dead center. The residual gas temperature T_R, in line with the simple approach followed in this paper, can be evaluated neglecting the heat transfer with in-cylinder wall during the exhaust stroke, thus assuming an isentropic transformation

$$T_R = T_4 \cdot \left(\frac{p_4}{p_S} \right)^{\frac{1 - k_S}{k_S}} \tag{A4}$$

where p_4 and T_4 are the in-cylinder gas pressure and temperature when the EVO. As mentioned, experimental findings confirmed by data reported in the scientific literature show that for a spark-ignition engine, the ratio T_4/T_1 ranges from 3.5 to 4.5. The isentropic coefficient k_S should be evaluated as a function of the exhaust gas composition and temperature, as described above (Eq. (25)).

References

[1] Leach, F., Kalghatgi, G., Stone, R., and Miles, P., 2020, "The Scope for Improving the Efficiency and Environmental Impact of Internal Combustion Engines," Transp. Eng., 1, p. 100005.
[2] Aghaali, H., and Ångström, H.-E., 2015, "A Review of Turbo Compounding as a Waste Heat Recovery System for Internal Combustion Engines," Renewable Sustainable Energy Rev., 49, pp. 813–824.
[3] Mamdouh, A., Fuhaid, A., and Apostolos, P., 2019, "Electric Boosting and Energy Recovery Systems for Engine Downsizing," Energies, 12(24), p. 4636.
[4] Gianluca, P., Giovanni, L., Stefano, F., Silvia, M., Massimo, C., Roberto, G., and Massimo, C., 2016, "Evaluation of an Electric Turbo Compound System for SI Engines: A Numerical Approach," Appl. Energy, 162, pp. 527–540.
[5] Ivan, A., Andrea, C., Cesare, P., Vincenzo, R., and De Cesare Mateo, D., 2015, "Evaluation of CO_2 Reduction in SI Engines With Electric Turbo-Compound by Dynamic Powertrain Modelling," IFAC-PapersOnLine, 48(15), pp. 93–100.
[6] Federico, M., Fabio, M., Enrico, P., and Ganio Mego, G., 2006, "The Potential of Electric Exhaust Gas Turbocharging for HD Diesel Engines," SAE Paper No. 2006-01-0437.
[7] Ulrich, H., and Algrain Marcelo, C., 2003, "Diesel Engine Electric Turbo Compound Technology," SAE Paper No. 2003-01-2294.
[8] Mohd Noor, A., Che Puteh, R., Rajoo, S., Basheer, U. M., Md Sah, M. H., and Shaikh Salleh, S. H., 2015, "Simulation Study on Electric Turbo-Compound (ETC) for Thermal Energy Recovery in Turbocharged Internal Combustion Engine," Appl. Mech. Mater., 799–800, pp. 895–901.
[9] Manuel, K., Alessandro, R., Mamat, B., Aman, M. I., and Ricardo, M.-B., 2015, "Heavy-Duty Engine Electric Turbocompounding," Proc. Inst. Mech. Eng., Part D: J. Automob. Eng., 229(4), pp. 457–472.
[10] Cipollone, R., Di Battista, D., and Gualtieri, A., 2013, "Turbo Compound Systems to Recover Energy in ICE," Int. J. Eng. Innovative Technol., 3(6), pp. 249–257.
[11] Lin, Z. W., Lei, H., Wei, W., Yangjun, Z., and Yongsheng, H., 2011, "Optimization of an Electric Turbo Compounding System for Gasoline Engine Exhaust Energy Recovery," SAE Paper No. 2011-01-0377.
[12] Ghosh, T. K., and Prelas, M. A., 2009, Energy Resources and Systems, Springer, Dordrecht, The Netherlands.
[13] Zhao, Y., and Chen, J., 2006, "Performance Analysis and Parametric Optimum Criteria of an Irreversible Atkinson Heat-Engine," Appl. Energy, 83(8), pp. 789–800.
[14] Hou, S.-S., 2007, "Comparison of Performances of Air Standard Atkinson and Otto Cycles With Heat Transfer Considerations," Energy Convers. Manage., 48(5), pp. 1683–1690.
[15] Zhao, J., and Xu, F., 2018, "Finite-Time Thermodynamic Modeling and a Comparative Performance Analysis for Irreversible Otto, Miller and Atkinson Cycles," Entropy, 20(1), p. 75.
[16] Miller, R. H., 1947, "Supercharging and Internal Cooling Cycle for High Output," Trans. ASME, 69, pp. 453–457.
[17] Kawamoto, N., Naiki, K., Kawai, T., Shikida, T., 2009, "Development of New 1.8-Liter Engine for Hybrid Vehicles," SAE Paper No. 2009-01-1061.
[18] Wang, Y., Lin, L., Zeng, S., Huang, J., Roskilly, A. P., He, Y., Huang, X., and Li, S., 2008, "Application of the Miller Cycle to Reduce NO_x Emissions From Petrol Engines," Appl. Energy, 85(6), pp. 463–474.
[19] Mi, C., and Abul Masrur, M., 2017, Hybrid Electric Vehicles: Principles and Applications With Practical Perspectives, 2nd ed., Wiley, Hoboken, NJ.
[20] Lars, E., Tobias, L., Oskar, L., and Andreas, T., 2012, "Scalable Component-Based Modeling for Optimizing Engines With Supercharging, E-Boost and Turbocompound Concepts," SAE Int. J. Engines, 5(2), pp. 579–595.
[21] Millo, F., Mallamo, F., Digiovanni, R., Dominici, A., Morel, T., and Okarmus, M., 2004, "Improving Misfire Diagnostic Through Coupled Engine/Vehicle Numerical Simulation," SAE Paper No. 2004-01-0613.
[22] Yuan, H., Chen, Z., Zhou, Z., Yang, Y., Brear, M. J., and Anderson, J. E., 2020, "Formulating Gasoline Surrogate for Emulating Octane Blending Properties With Ethanol," Fuel, 261, p. 116243.
[23] National Institute of Standards and Technology, 2022, "NIST Chemistry WebBook," National Institute of Standards and Technology, U.S. Department of Commerce, Gaithersburg, MD, accessed Feb. 10, 2022, https://webbook.nist.gov/chemistry/
[24] Andrew, H., and Andy, D., 2014, "Development of an Exhaust Driven Turbine-Generator Integrated Gas Energy Recovery System (TIGERS®)," SAE Paper No. 2014-01-1873.
[25] Michon, M., Calverley, S. D., Clark, R. E., Howe, D., Chambers, J. D. A., Sykes, P. A., Dickinson, P. G., 2007, "Modelling and Testing of a Turbo-Generator System for Exhaust Gas Energy Recovery," Proceedings of the 2007 IEEE Vehicle Power and Propulsion Conference, Arlington, TX, Sept. 9–12, Paper No. 4544184, pp. 544–550.
[26] Nonthakarn, P., Ekpanyapong, M., Nontakaew, U., and Bohez, E., 2019, "Design and Optimization of an Integrated Turbo-Generator and Thermoelectric Generator for Vehicle Exhaust Electrical Energy Recovery," Energies, 12(16), p. 3134.
[27] Beccari, S., and Pipitone, E., 2019, "Performance and Combustion Analysis of a Supercharged Double-Fuel Spark Ignition Engine," AIP Conf. Proc., 2191, p. 020017.
[28] Pipitone, E., and Beccari, A., 2007, "A Study on the Use of Combustion Phase Indicators for MBT Spark Timing on a Bi-Fuel Engine," SAE Paper No. 2007-24-0051.